

Radio Weak Lensing Shear Measurement in the Visibility Domain - II. Source Extraction

M. Rivi^{1*}, L. Miller²

¹*Department of Physics and Astronomy, University College London, Gower Street, London, WC1E 6BT, UK*

²*Astrophysics, Department of Physics, University of Oxford, Keble Road, Oxford, OX1 3RH, UK*

14 December 2024

ABSTRACT

This paper extends the method introduced in Rivi et al. (2016b) to measure galaxy ellipticities in the visibility domain for radio weak lensing surveys. In that paper we focused on the development and testing of the method for the simple case of individual galaxies located at the phase centre, and proposed to extend it to the realistic case of many sources in the field of view by extracting visibilities of each source with a facetting technique, taking into account the contamination from the other sources. In this second paper we present a detailed algorithm for source extraction in the visibility domain and show its effectiveness as a function of the source number density by running simulations of SKA1-MID observations in the band 950–1150 MHz and comparing original and measured values of galaxies’ ellipticities. Shear measurements from a realistic population of 10^4 galaxies randomly located in a field of view of 1 deg^2 (i.e. the source density expected for the current radio weak lensing survey proposal with SKA1) are also performed. At $\text{SNR} \geq 10$, the multiplicative bias is only a factor 1.5 worse than what found when analysing isolated sources, and is still comparable to the bias values reported for similar measurement methods at optical wavelengths. The additive bias is unchanged from the case of isolated sources, but is significantly larger than typically found in optical surveys. This bias depends on the shape of the Point Spread Function (PSF) and we suggest that a uv-plane weighting scheme to produce a more isotropic PSF could reduce and control additive bias.

Key words: gravitational lensing: weak - cosmology: observations - methods: statistical - techniques: interferometric

1 INTRODUCTION

Cosmological or targeted surveys of weak gravitational lensing at radio wavelengths may have a relevant role in the next years, when the Square Kilometre Array (SKA)¹ radio telescope will start to operate, providing a density of detected galaxies sufficient for shear measurement and a resolution to reliably measure their shapes. Radio observations have the advantage of a deterministic knowledge of the PSF and will provide unique approaches that are not available at the optical band, such as concurrent measurements of polarization and galaxy rotation velocities, that may be used to mitigate some of the astrophysical systematic effects such as intrinsic alignments. They may also be able to probe to higher redshifts given the different redshift distributions compared to the optical band (Brown et al. 2015). Being subject to different systematics, cross-correlation with optical surveys

will also allow suppression of systematic errors (Brown et al. 2015), improving shear measurement accuracy. Precursor radio weak lensing surveys such as SuperCLASS² and VLASS³ (Brown et al. 2013) are already underway and will soon provide data that may be used to test new methods required for galaxy shape measurement in the radio band. A natural approach for such methods is working in the visibility domain where the data originates and the noise is Gaussian, avoiding non-linear data manipulation of the imaging process. SKA simulations have already shown that current imaging methods produce images with structures in the residuals which may dominate the cosmological signal (Patel et al. 2015). Also cross-correlation analysis using real data images shows that no evidence of correlation is found between the optical and radio intrinsic shape of the matched objects (Patel et al. 2010; Tunbridge et al. 2016). This result suggests the presence of systematics in the procedure adopted for turning the

* E-mail: m.rivi@ucl.ac.uk

¹ <https://www.skatelescope.org>

² <http://www.e-merlin.ac.uk/legacy/projects/superclass.html>

³ <https://science.nrao.edu/science/surveys/vlass>

visibility data into images, although a significant percentage of AGN sources in the observed population may be another possible explanation.

Currently, cosmic shear in the radio band has been successfully detected only working in the visibility domain but obtaining sources position from the image (Chang et al. 2004). Galaxies' ellipticities from the VLA FIRST survey (Becker et al. 1995) were measured by decomposing them into shapelets, an orthonormal basis of functions corresponding to perturbations around a circular Gaussian invariant under Fourier transform (Chang & Refregier 2002). Since the number of resolved sources per beam is very small: $\sim 20 - 30 \text{ deg}^{-2}$, a joint fitting of the shapelet coefficients was possible by solving normal equations. Such an approach, computationally convenient, becomes very difficult when dealing with 10^4 sources per square degree, as expected from SKA Phase 1 continuum surveys (Brown et al. 2015). Moreover shapelets introduce a shear bias as they cannot accurately model steep brightness profiles and highly elliptical galaxy shapes (Melchior et al. 2010).

In Rivi et al. (2016b), we presented *RadioLensfit*, an alternative method working in the visibility domain where model fitting is performed on a single source at a time using an exponential profile as model for the galaxy. It is an adaptation of the optical Bayesian *lensfit* method (Miller et al. 2013) to radio data, where model visibilities are defined analytically and the likelihood is marginalised over uninteresting parameters. The method was tested and the shear bias estimated as function of the signal-to-noise ratio (SNR) in the simple case of individual galaxy visibilities, simulated with the SKA1-MID baseline configuration.

In this paper we extend this work implementing the method for extracting source visibilities from realistic data, i.e. when many galaxies are in the field of view. We estimate its effectiveness in terms of ellipticity fitting and shear measurement by running SKA1-MID simulations as we did in the previous paper. We finally investigate the effect of the PSF shape on the additive shear bias. This paper is organised as follows. In Section 2 we summarise *RadioLensfit* and present the extraction algorithm. In Section 3 details of SKA1 simulations are provided, while in Sections 4 and 5 results for galaxy ellipticity and shear measurements are presented respectively. Finally we discuss the shear additive noise bias in Section 6.

2 OVERVIEW OF RADIOLENSFIT

RadioLensfit is a method for measuring radio galaxy ellipticities in the visibility domain. The idea is to adapt the approach used in the optical case to radio data, i.e. extracting from visibilities and model fitting a single source at a time. Source extraction is difficult in the Fourier domain because signals from all sources in the beam are mixed altogether in the visibilities and sources are no longer localised. For this reason a joint analysis with the image domain may be needed: it allows us to identify sources and measure their position and flux with sufficient accuracy. With such information we can also compute a model of the observed sky and use it to approximate the signal from the other galaxies that must be removed when extracting each source. The extraction is completed using a faceting technique that phase

shifts the phase centre to the source position and further reduces its signal contamination by averaging visibilities in a coarse grid. Finally the model fitting can be performed as for the simple case of a single galaxy in the beam located at the phase centre as summarised in Section 2.1. This way we can largely reduce the computational time when a huge number of sources are in the field of view (as for SKA) instead of trying a challenging joint fitting of all sources. A detailed algorithm for the fitting of many sources in the beam visibilities is presented in Section 2.2.

2.1 Galaxy ellipticity fitting

In Rivi et al. (2016b) we introduced this method as an adaptation of *lensfit* (Miller et al. 2013) by performing the chi-square fitting of single source visibilities. They are evaluated at the uv points, that are defined by the baselines formed between two antennae projected on the plane orthogonal to the pointing direction. Model visibilities of a star-forming (SF) galaxy are computed analytically as the Fourier transform of the exponential brightness profile (Sérsic index $n = 1$):

$$V(u, v) = \left(\frac{\lambda_{\text{ref}}}{\lambda} \right)^\beta \frac{S_{\lambda_{\text{ref}}} e^{2\pi i(ul + vm)}}{(1 + 4\pi^2 \alpha^2 |\mathbf{A}^{-T} \mathbf{k}|^2)^{3/2}}, \quad (1)$$

where $\mathbf{k} = (u, v)^T$ is measured in wavenumber units, $\beta = -0.7$ is the assumed spectral index for the synchrotron radiation emitted by the galaxy disc, (l, m) and α are the source position and scalelength respectively, $S_{\lambda_{\text{ref}}}$ is the source flux at reference wavelength λ_{ref} . The ellipticity parameters (e_1, e_2) are contained in the matrix \mathbf{A} that linearly transforms the circular exponential profile to an ellipse:

$$\mathbf{A} = \begin{pmatrix} 1 - e_1 & -e_2 \\ -e_2 & 1 + e_1 \end{pmatrix}. \quad (2)$$

We assume the following ellipticity definition:

$$\mathbf{e} = e_1 + ie_2 = \frac{a - b}{a + b} e^{2i\theta}, \quad (3)$$

where a and b are the galaxy major and minor axes respectively, and θ is the galaxy orientation.

The likelihood is marginalised over non-interesting parameters such as flux, scalelength and position, adopting uniform priors for the flux and position and a lognormal prior dependent on the flux for the scalelength (Rivi et al. 2016a). This way we get a likelihood function of only the ellipticity parameters. The galaxy ellipticity measurement is given by the likelihood mean point and 1D standard deviation (defined as the square root of the covariance matrix determinant), obtained after sampling the likelihood with an adaptive grid covering a neighbourhood around the maximum point.

In real observations the finite channel bandwidth and sampling time introduce smearing effects that are dependent on the source position (Bridle & Schwab 1999). These effects may be approximated analytically and included in the visibilities model (Chang et al. 2004; Smirnov 2011). For example for frequency smearing:

$$\tilde{V}(u, v) = V(u, v) \text{sinc}[\pi(ul + vm)\Delta\nu/(\nu_0 c)], \quad (4)$$

where uv coordinates are taken at the mid-channel frequency ν_0 , $\Delta\nu$ is the channel bandwidth and $\text{sinc}(x) = \sin(x)/x$. Another option is to make the observation with

very tiny frequency channels and sampling time intervals. Harrison & Brown (2015) proposed to use ~ 30 kHz channel bandwidth and 0.5 s sampling time to make smearing tolerable, but meaning a huge number of uv points. In this case, raw visibilities may be averaged into a single uv grid without jeopardizing ellipticity measurements. In fact, observations from the same pair of antennae at different frequencies (resp. times) correspond to visibilities evaluated at different uv points along a radial (resp. tangential) direction, therefore these visibilities can be treated as the ones evaluated at uv points related to different baselines. Depending on the grid size, data volume and then computational time may be considerably reduced.

2.2 Source extraction

We assume flux and source positions are provided, for example they may be estimated from a cleaned image of the same data that are analysed, or applying MC methods to the visibilities (e.g. MultiNest⁴). From this information we define an initial sky model where the visibilities of each source s in the field of view are computed according to equation (1) with ellipticity $\mathbf{e} = (0, 0)$, i.e. circular source, and scalelength provided by the linear relation between the log of the median scalelength α_{med} and flux density S (Rivi et al. 2016a):

$$\ln[\alpha_{\text{med}}/\text{arcsec}] = -0.93 + 0.33 \ln[S/\mu\text{Jy}]. \quad (5)$$

The sky visibilities are obtained adding the model visibilities of each source in the beam:

$$V_{\text{sky}}(u, v) = \sum_{s=1}^N V_s(u, v). \quad (6)$$

Starting from this sky model, the source extraction and fitting procedure is performed according to decreasing flux order, i.e. decreasing SNR, as follows:

1. Given the position of the source (l, m) , remove the corresponding circular source model visibilities from the sky model and then take the difference between the data and the sky model, so that the visibilities of the current source (with a reduced contamination from the others) are extracted.
2. Apply *faceting* (Cornwell & Perley 1992): phase shift these visibilities in order to move the phase centre to the location of the source, by multiplying each visibility by the factor $\exp(-2\pi i(ul + vm))$, and average them in a coarse grid (facet). This way we reduce the field of view to a small patch around the source, with the advantage of reducing the number of visibilities used for the model fitting and therefore accelerating the computation. On the other hand this procedure limits the maximum wavelength of Fourier mode that can be measured because of the finite spacing of the facet uv points.
3. Use the extracted source visibilities for measuring the corresponding source ellipticity as in Section 2.1.
4. Use the estimated ellipticity to improve model visibilities of the current source and remove them from the data.
5. Repeat from step 1 until all sources are fitted.

Note that in this algorithm the sky model is improved after each source fitting by replacing circular sources with the

elliptical source that has been fitted. Moreover, by ordering the source extraction by decreasing flux, the source fitting is performed with a better approximation of the sky model for sources at low SNR.

In case of likelihoods that are too noisy⁵, corresponding sources are not removed in the first instance from the data and sky model visibilities, but they are re-fit at the end of the procedure when the ellipticities of all the other sources are measured and a better sky model is obtained. This happens when the computed likelihood has a too small standard deviation to be realistic. We refer to them as bad measurements.

3 SKA1 SIMULATIONS

As in the first paper, we simulate SKA-MID 8-hour observations of 1 square degree at declination $\delta = -30^\circ$ by using the SKA-MID⁶ Phase 1 antennae configuration provided in Heystek (2015). This integration time provides a complete circular coverage, i.e. without large gaps (because of the 3 telescope arms), and allow to reach a sensitivity of $10\mu\text{Jy}$ at 10σ . It would allow a targeted area of 800deg^2 to be observed with such sensitivity in 10,000 hours in a forthcoming SKA1 radio weak lensing survey, sufficient for measuring cluster lensing.

Visibilities are sampled every $\tau_{\text{acc}} = 60$ s in the first 30% of Band 2, i.e. 950 - 1190 MHz, considering one large channel as we don't include smearing effects on shorter time and bandwidth scales. The observations are simulated by using equations (1) and (6) and adding an uncorrelated Gaussian noise whose variance is given by Wrobel & Walker (1999):

$$\sigma^2 = \frac{\text{SEFD}^2}{2\eta^2 \Delta\nu \tau_{\text{acc}}}, \quad (7)$$

where $\Delta\nu$ is the frequency channel bandwidth, $\text{SEFD} = 400$ Jy is the system equivalent flux density for SKA-MID antennas and $\eta = 0.9$ is the system efficiency (Braun 2014). For simplicity we assume that the SKA1-MID core is composed of only SKA dish antennae even if part of it actually contains 64 MeerKAT dishes.

Source flux and scalelength are generated according to the distributions estimated in Rivi et al. (2016a) from the VLA-SWIRE radio source catalog. The modulus e of the intrinsic ellipticities is generated according to a function proposed by Miller et al. (2013):

$$P(e) = \frac{Ne(1 - \exp[-\frac{e - e_0}{c}])}{(1 + e)(e^2 + e_0^2)^{1/2}}, \quad (8)$$

but with the following parameter values: $c = 0.2298$, $e_0 = 0.0732$ and normalisation factor $N = 2.595$, obtained by fitting data from the VLA-COSMOS 1.4 GHz survey (Tunbridge et al. 2016). We generate SF galaxy populations with flux densities ranging between $10\mu\text{Jy}$ and $200\mu\text{Jy}$. According to our flux distribution we obtain a source number density of 2.7gal/arcmin^2 . To be consistent, we adopt this source number density in our simulation, although more accurate

⁴ <https://ccpforge.cse.rl.ac.uk/gf/project/multinest/>

⁵ By noisy likelihood we mean likelihood functions not sufficiently smooth to provide a reliable measurement, due to PSF sidelobes or too noise in the data.

⁶ SKA-MID latitude is $-30^\circ 49' 48.00''$ S.

S [μ Jy]	n. cells	best-fit slope	
		e_1	e_2
200-150	600	0.9774 ± 0.0025	0.9675 ± 0.0025
150-100	550	0.9795 ± 0.0030	0.9664 ± 0.0030
100-80	500	0.9797 ± 0.0032	0.9660 ± 0.0032
80-60	460	0.9774 ± 0.0029	0.9614 ± 0.0029
60-40	420	0.9760 ± 0.0031	0.9631 ± 0.0031
40-20	350	0.9756 ± 0.0028	0.9557 ± 0.0029
20-10	280	0.9765 ± 0.0030	0.9510 ± 0.0030

Table 1. Facet size dependent on source flux range and corresponding best-fit slope for 1000 sources.

modellings from recent radio continuum surveys suggest that a higher source number density should be detected at such a flux density cut in real observations (Condon et al. 2012; Mancuso et al. 2017).

4 GALAXY SHAPE MEASUREMENT

In this section, first we select the facet size to be used in the source extraction by simulating visibilities of individual sources. Then we simulate populations of galaxies located simultaneously in the field of view in order to show the efficacy of our source extraction algorithm as a function of the source number density.

4.1 Facet size

To minimise the number of sources falling in the same facet, we define a facet size dependent on source flux, as it is related to the size of the source. We split the flux total range of the simulated population, i.e. 10-200 μ Jy, in 7 bins. Facet uv point coordinates have to be re-computed only once per bin as the model fitting is performed according to source flux order. We chose larger bins at large fluxes because the sizes of such sources increase more gradually with the flux compared to the ones with low flux (see equation (5)). To estimate the facet size for each bin, we simulate raw visibilities of a single galaxy in the beam in order to avoid any source contamination effects, and vary the noise added to the visibilities (to have $\text{SNR} \geq 100$) in order to see the effect of the source size only. We measure the galaxy ellipticity after averaging visibilities in the facet. A relatively large facet size is expected even for covering a single galaxy because of the source convolution with a large sized PSF (see Fig. 1). In fact the PSF corresponding to the original uv coverage, where uv points have natural weighting, has a broad, low-level plateau because uv points have short spacings close to zero, as they tend to spend more time per unit area near the uv origin. This means that a large contribution to the signal is from short baselines which must be adequately sampled.

The best-fit line slope for the ellipticity measurements of 1000 galaxies is computed for different facet sizes and source flux ranging between the flux bin bounds. We select the facet size when a fixed best-fit slope threshold of about 0.97 is reached, as listed in Tab. 1. Notice that the fitting for the first ellipticity component is better than the second one because of a slightly anisotropy of the PSF as discussed in Sect. 6. The selected facets size are consistent with the

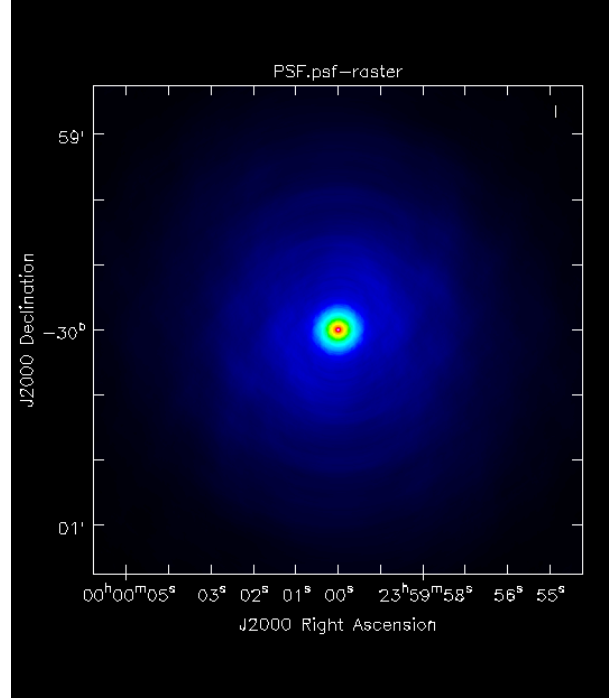


Figure 1. Image of the PSF corresponding to our SKA1 uv coverage. Its FWHM is about 9 arcsec.

relation between the uv grid cell size Δu (in units of wavelengths) and the related field of view (in radians): f.o.v. = $1/\Delta u$ (Briggs et al. 1999). We also noticed that for small sources (low flux) it is actually better to use smaller facet even in the case of single source in the field of view. This is shown in Fig. 2 where binned measurements of the first ellipticity component of 1000 galaxies, with realistic flux distribution in the range 10-200 μ Jy, are plotted both for the case where the facet size is constant and equal to 600 (top panel) and when the facet has a variable size dependent on the source flux (bottom panel). Similar plots are obtained for the second component. In the latter the number of bad measurements is about 3 times smaller and the best-fit slope of the two ellipticity components are 0.9552 ± 0.0057 and 0.9426 ± 0.0061 respectively, whereas for the case of 600×600 facet the best-fit lines slopes for the same galaxy population and noise is 0.9360 ± 0.0056 and 0.9094 ± 0.0059 .

These results are due to the fact that we do not model exactly the beam because the model visibilities are directly sampled on the uv facet points. This means that in the image domain the sidelobes of the source model are not suppressed by any apodisation, whereas the gridding of the original uv coverage causes the full image to be apodised by a broad 2D sinc function which has the effect in the data of suppressing background sources that are a long way from the phase centre and the distant sidelobes from the primary source. The grid sampling causes the resulting image domain facet to become a small, but aliased version of the apodised image. The aliased model is an incorrect description of the apodised and aliased data, and the discrepancy will get worse for smaller facets. The bias this introduces might coincidentally offset some other bias such as noise bias, but such offsetting of biases is not robust to changes in the galaxy population or observing setup, so it is not desirable. We could improve the

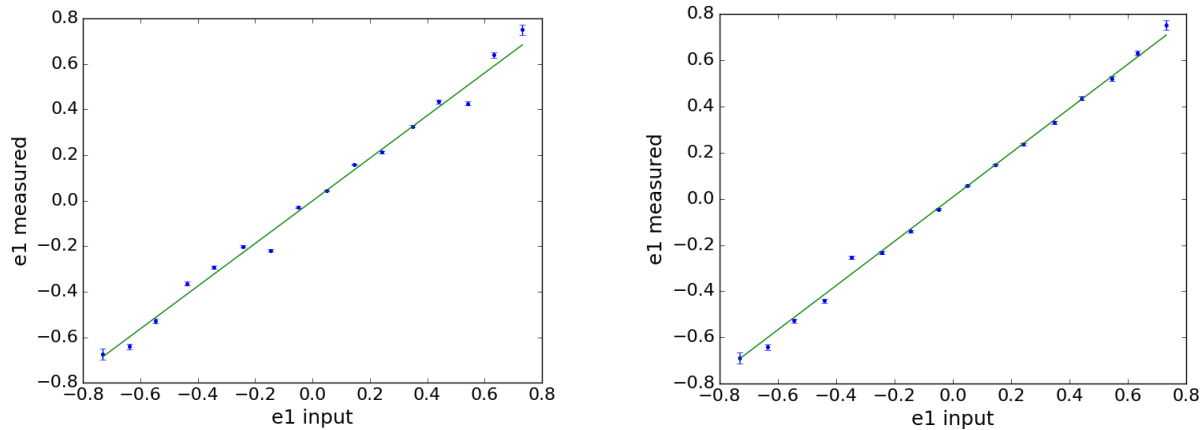


Figure 2. Best-fit line slopes for binned measurements of the ellipticity first component of 1000 individual galaxies randomly located in the field of view and with flux ranging between $10 \mu\text{Jy}$ and $200 \mu\text{Jy}$. *Left:* facet size 600×600 for all sources. *Right:* facet size dependent on source flux.

model by applying the same gridding operations as in the data (sampling on the original uv coverage and then averaging in the facet), but this will add a large amount of computational time. Our results show that the adopted model approximation is acceptable, provided that the facet sizes are sufficiently large to not affect the significant sidelobes in the image domain. Otherwise we expect the discrepancy between data and model to become severe and the biases may become less robust and hence less calibratable.

4.2 Dependency on source number density

We estimate the efficacy of the source extraction method by measuring the slope of the best-fit lines of galaxy ellipticity measurements as a function of the source number density. For each measurement we simulate sources located simultaneously in the primary beam according to a uniform distribution. Results are plotted in Fig. 3 and show reliable fits, independent of the source density up to 2.8 gal/arcmin^2 . In this case the best-fit line slope of the two ellipticity components are 0.9365 ± 0.0017 and 0.9262 ± 0.0017 respectively and the number of bad measurements is about 1%. At higher densities galaxy ellipticity measurement starts to deteriorate, as residuals of nearby galaxies affect the model fitting, but may still be good enough for shear measurement. Otherwise galaxies within facets, which will be a relatively small number, may be jointly fitted, making this approach more feasible. Joint fitting can be performed by applying the HMC technique (Neal 2011). Preliminary results with this method show a better accuracy in the galaxy ellipticity fitting, although requiring a much larger computational time (Rivi et al., in preparation). Results obtained with *RadioLensfit* can be used as starting points for the Markov chains in order to reduce the burn-in phase and accelerate convergence.

5 SHEAR

Following Rivi et al. (2016b), for shear measurement we simulate a SKA1 source density as described in Sect. 3, corre-

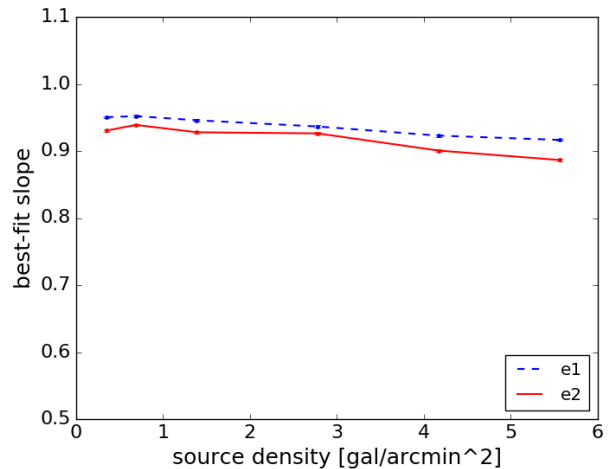


Figure 3. Best-fit line slope for both galaxy ellipticity components as a function of the source number density.

sponding to a population of 10^4 galaxies in a field of view of 1 deg^2 . We generate a population free of shape noise (Nakajima & Bernstein (2007); Massey et al. (2007)): for each ellipticity modulus, 10 equally-spaced galaxy orientations are generated so that the corresponding ellipticity values are distributed uniformly on a circle, and galaxies whose ellipticity is on the same ring are given the same size and flux. We generate sources randomly located according to a uniform distribution and compare results with the optimal case where each galaxy is at the phase centre and the only one contained in the field of view. All measurements are performed with faceting size dependent on the source flux as defined in Table 1.

We measure the reduced shear $\mathbf{g} = g_1 + ig_2$ as the weighted average of the galaxies' ellipticities using weights that approximate the inverse-variance of each ellipticity measurement. Error bars are given by the standard deviation of the shear values estimated from 1000 bootstrap re-

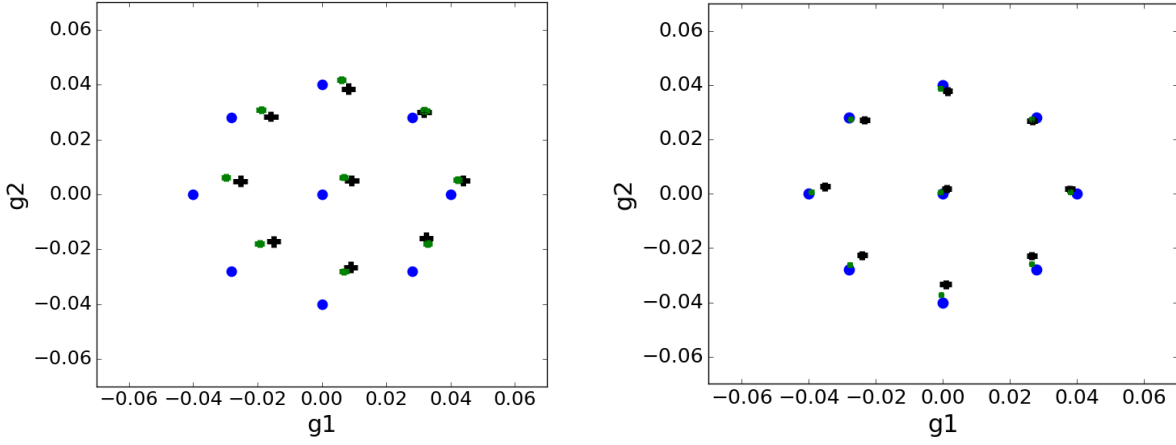


Figure 4. Comparison of shear measurements: input values are blu points, measured values from single sources at the phase centre are green crosses, measured values from sources simultaneously in the f.o.v are black crosses. *Left*: $\text{SNR} \geq 10$. *Right*: $\text{SNR} \geq 25$.

	g_1	g_2
single source	0.00932 ± 0.00233	0.00497 ± 0.00200
multiple sources	0.00676 ± 0.00146	0.00627 ± 0.00138

Table 2. Measured shear components for input $\mathbf{g} = 0$.

samples. When no shear is applied, i.e. $g_1 = g_2 = 0$, the shear measured in the optimal case of individual source visibilities and the real case of multiple sources in the field of view is showed in Table 2, considering the same galaxy population.

We repeat such a comparison for other input reduced shear values with amplitude $g = 0.04$ and eight different orientations. The input shear \mathbf{g} action on the intrinsic galaxy ellipticity \mathbf{e}^s is simulated following Seitz & Schneider (1997):

$$\mathbf{e} = \frac{\mathbf{e}^s + \mathbf{g}}{1 + \mathbf{g}^* \mathbf{e}^s}, \quad (9)$$

where \mathbf{g}^* is the shear complex conjugate. Results are plotted in Fig. 4, both for $\text{SNR} \geq 10$ and $\text{SNR} \geq 25$, where measurements from individual source visibilities are green crosses and the ones from the same population but with all sources simultaneously in the beam are black crosses. Clearly error bars (cross arms) are larger at $\text{SNR} \geq 10$.

The measured shear bias, defined as

$$g_i^m - g_i = m_i g_i + c_i, \quad i = 1, 2, \quad (10)$$

is showed in Table 5. At $\text{SNR} \geq 10$, the multiplicative biases m_i for the two shear components are respectively 1.6 and 1.4 times the ideal case of a single source in the field of view, while additive bias c_i are almost consistent.

The source signal contamination by residuals of nearby galaxies is a new contribution to the shear bias that seems to have a larger effect on the multiplicative term, in fact it does not decrease much at higher SNR. This effect may be mitigated by refining ellipticity measurements by joint fitting within larger facets, as explained in Sect. 4.2. These bias values are comparable to the ones obtained from optical surveys using *lensfit* (Fenech Conti et al. 2017) and *im3shape*

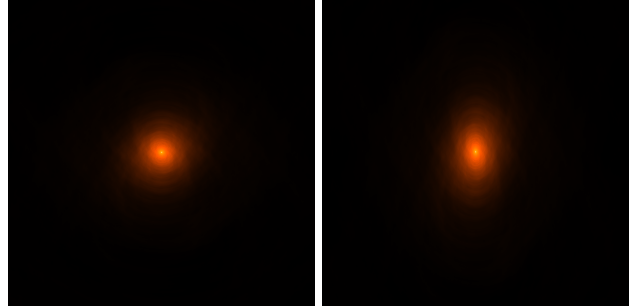


Figure 5. *Left*: PSF corresponding to the original declination (zenith). *Right*: PSF corresponding to a declination increased by 50° , neglecting the earth rotation.

(Zuntz et al. 2017)), where measurements calibration is required as discussed in Rivi et al. (2016b). Currently the best method in the optical domain designed to calibrate standard shear estimators is *Metacalibration* (Huff & Mandelbaum (2017); Sheldon & Huff (2017)) which is used in the analysis of the Dark Energy Survey⁷ (DES) (Zuntz et al. 2017). This method applies a self-calibration at the time of the measurement which reduces the multiplicative bias in simulations to well below the percent level. It also isotropises the PSF to remove any additive bias. A similar approach may be implemented quite easily in the interferometer data analysis, with the advantage that for the additive bias at radio wavelengths we know the PSF much better than at optical wavelengths and we can make the PSF isotropic directly by weighting the uv-plane (as discussed in Sect. 6).

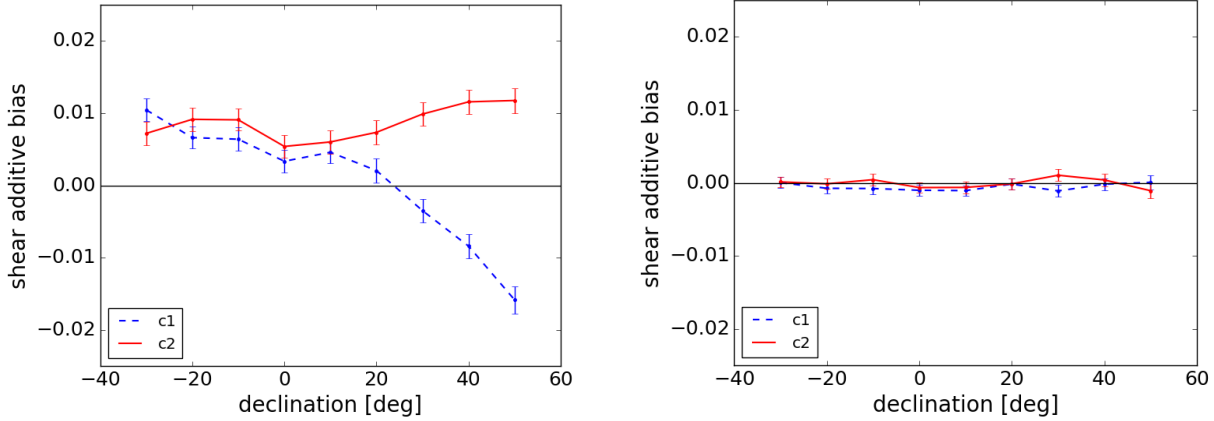
6 ADDITIVE BIAS DEPENDENCE ON THE PSF SHAPE

It is well known from weak lensing optical surveys that shear additive bias is dependent on the PSF shape (Miller et al.

⁷ <https://www.darkenergysurvey.org>

		m_1	c_1	m_2	c_2
SNR ≥ 10	single source	-0.0904 ± 0.0186	0.00655 ± 0.00050	-0.1297 ± 0.0171	0.00632 ± 0.00046
	multiple sources	-0.1428 ± 0.0274	0.00872 ± 0.00073	-0.1864 ± 0.0256	0.00578 ± 0.00067
SNR ≥ 25	single source	-0.0348 ± 0.0091	-0.00064 ± 0.00024	-0.0473 ± 0.0088	0.00076 ± 0.00023
	multiple sources	-0.0941 ± 0.0196	0.00135 ± 0.00053	-0.1098 ± 0.0194	0.00214 ± 0.00051

Table 3. Shear noise bias.

Figure 6. Shear additive bias as a function of the source declination. The zenith corresponds to $\delta = -30^\circ$. Facet size fixed at 800×800 . Left: SNR ≥ 10 . Right: SNR ≥ 25 .

(2013)). For radio interferometers the PSF is deterministically defined by the uv coverage of the telescope (i.e. antennae locations and pointing direction). For example, if we increase the antenna pointing declination of a given angle the PSF shape turns to be compressed along the y-axis (see Fig. 5).

We measure the additive noise bias for different source declinations at different SNR values. Starting from our uv coverage, we simulate the phase centre declination increment of an angle ϕ by rotating the uv plane about the u axis, therefore only v coordinates change as $v' = v \cos(\phi)$. This is a simple and pessimistic approximation of this effect on the beam ellipticity because we should have also considered that in such a long integration time the source position is moving because of the rotation of the earth. We simulate individual source visibilities, to avoid nearby source contamination effects, and assume a constant maximum facet size 800×800 to ensure that the galaxy convolved with the PSF is entirely contained in the facet even when the PSF becomes highly anisotropic.

We observe that the additive bias is dependent on source sizes. In fact measurements at the same SNR obtained by lowering the noise instead of increasing the source flux cut, produce larger bias values, meaning that the additive bias worsens when source sizes decreases. This is consistent with the analysis presented in Massey et al. (2013). Noise bias causes a correlation between measured shear and PSF ellipticity even when we correct for the PSF in the model fitting. This becomes noticeable at low SNR, where the first ellipticity component increases significantly towards larger negative values, as the PSF becomes more and more

compressed along the y direction (see left panel of Fig. 6). At large SNR the additive bias almost disappears independently of the PSF shape (see right panel of Fig. 6). This is in good agreement with what we should expect. Because of our long integration time the PSF is not isotropic even when the declination equals the observatory latitude, as in the baseline simulation, besides the fact that the distribution of the SKA-MID baselines on the ground may not be circularly symmetric. Therefore a large additive bias is still measured at declination values closed to the zenith. Usually the PSF isotropy is controlled by the choice of the observation times, which are small time intervals distributed along the year. However this may not be sufficient to reach an additive bias acceptable for weak lensing surveys. To further reduce the noise bias at low SNR we also need to weight the uv plane to ensure that the PSF is more isotropic. A standard technique in radio imaging to improve PSF shape is to use tapering functions (Briggs et al. 1999) to define uv points weights, although a more specific weighting scheme may be required. Moreover, as for the multiplicative bias, we can calibrate the additive shear bias with simulations. This is more feasible than in optical surveys because the PSF is deterministic at radio wavelengths. However, any such calibration would be strongly dependent on distributions of source properties, so isotropising the PSF is a much better option.

Notice that when using variable size faceting, the facet size must be dependent not only on the source size but also on the PSF shape. In fact as the PSF becomes anisotropic the facet size may become too small relative to the size of the source modifying the effective shape of the source. For example the left panel of Fig. 7 shows what happens at

$\text{SNR} \geq 10$ when we maintain the same flux dependent facets size (Table 1) for all pointing declinations: at large zenith distances the shortest baselines occupy smaller uv frequencies and therefore can measure wavelengths longer than the limit imposed by a the small facet size used to extract the majority of the galaxy population. If we increase the facets size according to the source declination we obtain consistent results with the case of one single large facet (see right panel of Fig. 7).

7 CONCLUSIONS

We have extended the presentation of the *RadioLensfit* method, introduced in Rivi et al. (2016b) for the simple case of individual galaxies located at the phase centre, to the real case where many galaxies are randomly located in the field of view. This has been done by extracting the visibilities of each source and shifting the phase centre to the source position so that a coarse grid can still be used to accelerate ellipticity measurement computation. Source extraction has been performed by removing from the data the simulated visibilities of the sky model, but the source of interest, given position and flux of all sources in the beam from the image, and down-weighting what remains of nearby sources contamination by averaging visibilities in the coarse grid (facet). For gridding we adopted a natural weighting to maximise sensitivity and estimated the smallest facet size dependent on source flux thresholds in order to minimise the number of nearby galaxy included in the grid.

We tested the source extraction procedure simulating visibilities of SF galaxy populations observed by SKA1-MID in the 30 per cent of frequency Band 2. We adopted flux and scalelength parameters distributions estimated from the VLA SWIRE catalog and used *lensfit* ellipticity prior with coefficients fitted from VLA COSMOS catalog.

We showed the efficacy of our source extraction algorithm as a function of the source number density, obtaining a reliable galaxy ellipticity fitting for the density expected from the current proposal of the SKA1 radio weak lensing survey. Shear measurements from 8-hour observation of one square degree show that the bias due to the extraction procedure mainly affects the multiplicative bias as no significant change has been observed for the additive bias when comparing with the bias obtained for the ideal case of a single source at the phase centre at a time. This bias may be mitigated by a second step in the galaxy ellipticity measurement, where a joint fitting within the facets is performed with HMC, starting from the values obtained with *RadioLensfit*. However multiplicative shear calibration is also required as for the optical domain.

We finally observed that because of our uv coverage the PSF is slightly anisotropic even if pointing close to the zenith, therefore we obtain a large additive bias. Although a suitable choice of the integration time (split and distributed along a longer period of time) actually reduces the PSF anisotropy, a uv weighting scheme may still be required to satisfy weak lensing requirements.

ACKNOWLEDGEMENTS

We thank Tom Kitching for useful discussions and Ben Tunbridge for providing the distribution parameters of our ellipticity prior, obtained by fitting VLA-COSMOS data as for the prior function presented in his paper.

MR acknowledges the support of the Science and Technology Facilities Council via an SKA grant. LM acknowledges STFC grant ST/N000919/1.

REFERENCES

- Becker R., White R., D.J.Helfand, 1995, ApJ, 450, 559
- Braun R., 2014, SKA Memo
- Bridle A., Schwab F., 1999, in ASP Conf. Ser., Vol. 180, Synthesis Imaging in Radio Astronomy II, Taylor G., Carilli C., Perley R., eds., Astron. Soc. Pac., San Francisco, p. 371
- Briggs D., Schwab F., Sramek R., 1999, in ASP Conf. Ser., Vol. 180, Synthesis Imaging in Radio Astronomy II, Taylor G., Carilli C., Perley R., eds., Astron. Soc. Pac., San Francisco, p. 129
- Brown M., Abdalla F. B., Amara A., Bacon D. J., Battye R. A., Bell M. R., Beswick R. J., Birkinshaw M. et al, 2013, preprint (arXiv:1312.5618)
- Brown et al. M., 2015, in Advancing Astrophysics with the Square Kilometre Array, Vol. 2, Proc. Sci., SISSA, Trieste, p. 1365
- Chang T., Refregier A., 2002, ApJ, 570, 447
- Chang T., Refregier A., Helfand D., 2004, ApJ, 617, 794
- Condon J., Cotton W., Domalont E., Kellermann K., Miller N., Perley R., Scott D., Vernstrom T. et al, 2012, AJ, 758, 23
- Cornwell T. J., Perley R. A., 1992, A&A, 261
- Fenech Conti I., Herbonnet R., Hoekstra H., Merten J., Miller L., Viola M., 2017, MNRAS, 467, 1627
- Harrison I., Brown M., 2015, SKA Engineering Change Proposal: Gridded Visibilities to Enable Precision Cosmology with Radio Weak Lensing. arXiv: 1507.06639
- Heystek L., 2015, SKA Memo
- Huff E., Mandelbaum R., 2017, ArXiv e-prints
- Mancuso C., Lapi A., Prandoni I., Obi I., Gonzalez-Nuevo J., Perrotta F., Bressan A., Celotti A. et al, 2017, AJ, 842, 95
- Massey R., Heymans C., Bergé J., Bernstein G., Bridle S., Clowe D., Dahle H., Ellis R. et al, 2007, MNRAS, 376, 13
- Massey R., Hoekstra H., Kitching T., Rhodes J., Cropper M., Amiaux J., Harvey D., Mellier Y. et al, 2013, MNRAS, 429, 661
- Melchior P., Böhnert A., Lombardi M., Bartelmann M., 2010, A&A, 510, A75
- Miller L., Heymans C., Kitching T. D., van Waerbeke L., Erben T., Hildebrandt H., Hoekstra H., Mellier Y. et al, 2013, MNRAS, 429, 2858
- Nakajima R., Bernstein G., 2007, ApJ, 133, 1763
- Neal R. M., 2011, MCMC using Hamiltonian dynamics, Brooks S., Gelman A., Jones G., Meng X.-L., eds., Chapman & Hall/CRC Press
- Patel P., Bacon D. J., Beswick R. J., Muxlow T. W. B., Hoyle B., 2010, MNRAS, 401, 2572
- Patel P., Harrison I., Makhathini S., Abdalla F., Bacon D.,

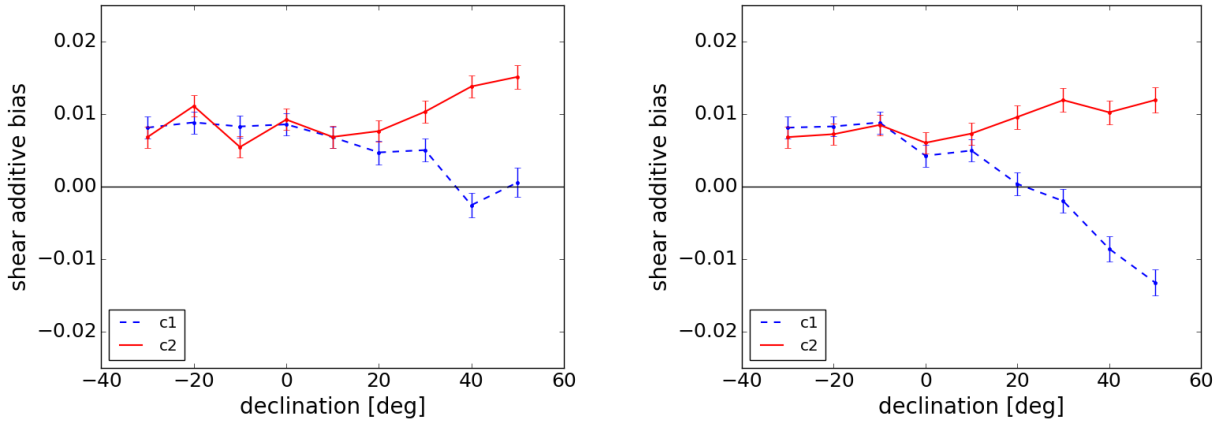


Figure 7. Shear additive bias at $\text{SNR} \geq 10$ as a function of the source declination. The zenith corresponds to $\delta = -30^\circ$. *Left:* facets size dependent on source flux according to Table 1 for all declinations. *Right:* facets size increased with source declination.

- Brown M., Heywood I., Jarvis M., Smirnov O., 2015, in Advancing Astrophysics with the Square Kilometre Array, Vol. 2, Proc. Sci., SISSA, Trieste, p. 1427
- Rivi M., Miller L., Makhathini S., Abdalla F., 2016a, in EXTRA-RADSUR2015, Proc. Sci., SISSA, Trieste
- Rivi M., Miller L., Makhathini S., Abdalla F. B., 2016b, MNRAS, 463, 1881
- Seitz C., Schneider P., 1997, A & A, 318, 687
- Sheldon E. S., Huff E. M., 2017, ApJ, 841, 24
- Smirnov O. M., 2011, A& A, 527, A106
- Tunbridge B., Harrison I., Brown M., 2016, MNRAS, 463, 3339
- Wrobel J., Walker R., 1999, in ASP Conf. Ser., Vol. 180, Synthesis Imaging in Radio Astronomy II, Taylor G., Carilli C., Perley R., eds., Astron. Soc. Pac., San Francisco, p. 171
- Zuntz J., Sheldon E., Samuroff S., Troxel M. A., Jarvis M., MacCrann N., Gruen D., Prat J. et al, 2017, ArXiv e-prints